AIP Journal of Applied Physics

High-pressure phase transitions and compressibility of wolframite-type tungstates

J. Ruiz-Fuertes, S. López-Moreno, D. Errandonea, J. Pellicer-Porres, R. Lacomba-Perales, A. Segura, P. Rodríguez-Hernández, A. Muñoz, A. H. Romero, and J. González

Citation: Journal of Applied Physics **107**, 083506 (2010); doi: 10.1063/1.3380848
View online: http://dx.doi.org/10.1063/1.3380848
View Table of Contents: http://scitation.aip.org/content/aip/journal/jap/107/8?ver=pdfcov
Published by the AIP Publishing

High-pressure phase transitions and compressibility of wolframite-type tungstates

J. Ruiz-Fuertes,[1] S. López-Moreno,[2] D. Errandonea,[3,a)] J. Pellicer-Porres,[1] R. Lacomba-Perales,[1] A. Segura,[1] P. Rodríguez-Hernández,[4] A. Muñoz,[4] A. H. Romero,[2] and J. González[5]

[1]*MALTA Consolider Team, Departamento de Física Aplicada—ICMUV, Universitat de València, Edificio de Investigación, c/Dr. Moliner 50, 46100 Burjassot, Valencia, Spain*
[2]*CINVESTAV-Querétaro, Libramiento Norponiente No 2000, Real de Juriquilla 76230 Querétaro, Mexico*
[3]*MALTA Consolider Team, Departamento de Física Aplicada—ICMUV, Fundación General de la Universitat de València, Edificio de Investigación, c/Dr. Moliner 50, 46100 Burjassot, Valencia, Spain*
[4]*MALTA Consolider Team, Departamento de Física Fundamental II, and Instituto de Materiales y Nanotecnología, Universidad de La Laguna, La Laguna 38205 Tenerife, Spain*
[5]*MALTA Consolider Team, DCITIMAC, Facultad de Ciencias, Universidad de Cantabria, 39005 Santander, Spain*

(Received 12 February 2010; accepted 10 March 2010; published online 23 April 2010)

This paper reports an investigation on the phase diagram and compressibility of wolframite-type tungstates by means of x-ray powder diffraction and absorption in a diamond-anvil cell and *ab initio* calculations. X-ray diffraction experiments show that monoclinic wolframite-type $MgWO_4$ suffers at least two phase transitions, the first one being to a triclinic polymorph with a structure similar to that of $CuWO_4$ and $FeMoO_4$-II. The onset of each transition is detected at 17.1 and 31 GPa. In $ZnWO_4$ the onset of the monoclinic-triclinic transition has been also found at 16.7 GPa. This transition does not involve any change in the atomic coordination as confirmed by x-ray absorption measurements. These findings are supported by density-functional theory calculations, which predict the occurrence of additional transitions upon further compression. Calculations have been also performed for wolframite-type $MnWO_4$, which is found to have an antiferromagnetic configuration. In addition, our study reveals details of the local-atomic compression in $MgWO_4$ and $ZnWO_4$. In particular, below the transition pressure the ZnO_6 and equivalent polyhedra tend to become more regular, whereas, the WO_6 octahedra remain almost unchanged. Fitting the pressure-volume data we obtained the equation of state for the low-pressure phase of $MgWO_4$ and $ZnWO_4$. These and previous results on $MnWO_4$ and $CdWO_4$ are compared with the calculations. The compressibility of wolframite-type tungstates is also systematically discussed. Finally Raman spectroscopy measurements and lattice dynamics calculations are presented for $MgWO_4$. © *2010 American Institute of Physics*. [doi:10.1063/1.3380848]

I. INTRODUCTION

Materials belonging to the tungstate family (AWO_4 with A being a divalent element) have a long history of practical application and have been the object of extensive research. Their optical and luminescence properties have received great attention as these compounds are widely used as scintillating detectors in high-energy particle physics, rare-event searches, and medical diagnosis among other applications.[1] From the fundamental and geophysical standpoints, AWO_4 oxides are also interesting compounds.[2] Tungstates of large divalent cations (Ca, Ba, Pb, Sr, and Eu) usually crystallize in the tetragonal scheelite structure (space group: $I4_1/a$, $Z=4$) and those compounds of small divalent cations (Cd, Zn, Mg, Mn, etc.) can take the wolframite structure (space group: $P2/c$, $Z=2$).[3] In wolframite (shown in Fig. 1), both A and W cations have octahedral oxygen coordination and each octahedron shares two corners with its neighbors.[4]

In the last years there has arisen renewed interest in AWO_4 compounds and their evolution under pressure. In the case of wolframites, high-pressure (HP) Raman spectroscopy studies have been performed in $CdWO_4$ (Refs. 5 and 6) and $ZnWO_4$ (the mineral sanmartinite).[7,8] *Ab initio* calculations have been also carried out to study their structural stability.[6,8] In $ZnWO_4$ a pressure-induced phase transition has been detected beyond 30 GPa (Ref. 8) and a subsequent transition suggested near 58 GPa. A monoclinic β-fergusonite-type structure (space group: $C2/c$, $Z=4$) has been proposed for the HP phase. In $CdWO_4$ two transitions take place around 20 and 35 GPa and two coexisting phases are found within this pressure range, one with tetragonal and another with triclinic symmetry. At 35 GPa $CdWO_4$ transforms to a

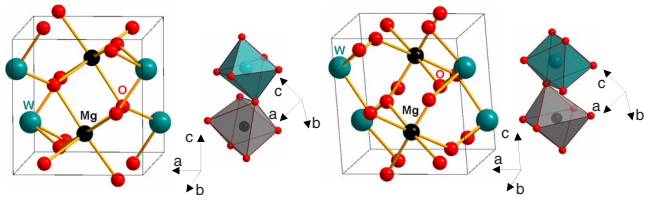

FIG. 1. (Color online) Schematic view of the wolframite structure with a detail of both octahedra (left) and of the $P\bar{1}$ triclinic structure (right).

a)Electronic mail: daniel.errandonea@uv.es.

β-fergusonite-type structure. Under the current status of the research, HP x-ray diffraction (XRD) studies are needed to further progress on the understanding of the structural properties of wolframites. However, in contrast with scheelite-structured tungstates,[1,9,10] such studies have been rarely performed in wolframites. Indeed $CdWO_4$, $MgWO_4$, and $MnWO_4$ (the mineral hübnerite) have been studied only up to a pressure lower than 8 GPa.[11] Therefore, the information available is limited to the compression of the wolframite phase at low pressures.

Motivated by the above-described facts, we have undertaken a comparative study of the structural properties of $CdWO_4$, $MgWO_4$, $MnWO_4$, and $ZnWO_4$ under compression. In this paper, we report HP angle-dispersive XRD (ADXRD) experiments in $MgWO_4$ ($ZnWO_4$) up to 50 (26) GPa as well as x-ray absorption spectroscopy (XAS) measurements in $ZnWO_4$ up to 18 GPa at the Zn K-edge. The obtained results are interpreted with the help of *ab initio* total-energy calculations. In $MgWO_4$, we observe two phase transitions and propose a triclinic structure for the first HP phase. For $ZnWO_4$ an intermediate phase with $P\bar{1}$ symmetry has been found at lower pressure than the proposed phase with $C2/c$ symmetry,[8] pointing toward the same sequence followed by $MgWO_4$. The equation of state (EOS) for the wolframite phase has been determined. Calculations performed for wolframite $CdWO_4$ and $MnWO_4$ are also compared with earlier data. In addition, lattice dynamics properties of $MgWO_4$ have been computed, being the Raman-active and infrared (IR)-active phonons and their pressure dependences determined. Finally, Raman measurements have been carried out for $MgWO_4$.

II. EXPERIMENTAL DETAILS

To perform the experiments we used micron-size powder samples with a purity higher than 99% (Aldrich). Their crystal structures at ambient conditions were checked by powder XRD using a Seifert XRD 3003 TT diffractometer with Cu $K_{\alpha 1}$ monochromatic radiation ($\lambda = 1.5406$ Å). The diffraction patterns of $MgWO_4$ and $ZnWO_4$ correspond to the wolframite-type phase with no indication of additional phases. The unit-cell parameters were $a=4.689(2)$ Å, $b=5.675(2)$ Å, $c=4.928(2)$ Å, and $\beta=90.75(5)°$ for $MgWO_4$ and $a=4.680(2)$ Å, $b=5.712(2)$ Å, $c=4.933(2)$ Å, and $\beta=90.30(5)°$ for $ZnWO_4$. The agreement is excellent with previous studies.[3,8,11]

ADXRD experiments were carried out at beamline I15 in the Diamond Light Source with a monochromatic x-ray beam ($\lambda=0.6118$ Å), which was focused down to 30×30 μm^2 using Kirkpatrick–Baez mirrors. In order to pressurize the samples two different diamond-anvil cells (DACs) were used: a membrane-type DAC with diamond-culets of 400 μm and a Boehler–Almax-type DAC with diamond-culets of 280 μm. In the membrane DAC, samples were loaded in 150-μm-holes drilled in Inconel gaskets and in the Boehler–Almax DAC in 100-μm-holes drilled in tungsten gaskets. Silicone oil was used as pressure-transmitting medium[12,13] and the pressure was measured by means of the ruby fluorescence technique.[14] A pinhole placed before the sample position was used as a clean-up aperture for filtering out the tail of the focused x-ray beam. High-resolution diffraction patterns were recorded using a MAR345 image plate located at a distance of 423 mm from the sample. They were integrated and corrected for distortions using FIT2D. The analysis and indexing of the structures was performed using POWDERCELL, DICVOL, UNITCELL, and GSAS. One experiment was carried out in $MgWO_4$ and two different runs were performed for $ZnWO_4$.

Dispersive x-ray absorption experiments on $ZnWO_4$ up to 18 GPa were carried out at ODE beamline in the Soleil Synchrotron using a membrane DAC with 400 μm-diameter diamond-culets. Experiments were conducted at the Zn K-edge (9.659 KeV) with a focused polychromatic beam of 50×50 μm^2 and using metallic Zn as a reference compound for energy calibration. The incident and transmitted beam were systematically measured using a grazing mirror between the sample and the charge coupled device (CCD) detector in order to avoid the presence of harmonics. The sample, in powder form (absorption jump of $\Delta\mu d\sim2.1$), was loaded in a 200 μm-diameter hole of an Inconel gasket, together with ruby chips and silicone oil as pressure-transmitting medium.

Unpolarized confocal micro-Raman scattering measurements were performed at room temperature in a triple monochromator Jobin-Yvon T64000 in the subtractive mode equipped with a liquid N_2 cooled CCD detector, in the backscattering geometry. For excitation, the 514.5 nm line of an Ar^+ laser (wavelengths longer than that of the $MgWO_4$ band gap[15]) was focused on the sample by means of a 100× objective, while the laser power was kept below 2 mW, in order to avoid laser-heating effects on the probed material and the concomitant softening of the observed Raman peaks. This was verified by varying the incident power and observing that neither the Stokes to anti-Stokes intensity ratio nor the frequency of the Ag mode at 916.8 cm^{-1} varied within experimental precision. The laser spot diameter on the sample was 1 μm and the spectral resolution was better that 1 cm^{-1}.

III. CALCULATIONS

First-principles total-energy and lattice-dynamics calculations were done within the framework of the density-functional theory (DFT) and the pseudopotential method using the Vienna *ab initio* simulation package (VASP).[16–18] The exchange and correlation energy was initially taken in the local-density approximation (LDA) (Ref. 19) for $MgWO_4$ and the generalized-gradient approximation (GGA) according to Perdew–Burke–Ernzerhof prescription for $MnWO_4$.[20] The projector-augmented wave (PAW) scheme[21,22] was adopted and the semicore 5*p* electrons of W were also explicitly included in the calculations. The set of plane waves used extended up to a kinetic energy cutoff of 520 eV. This large cutoff was required to deal with the O atoms within the PAW scheme to ensure highly converged results. The Monkhorst–Pack (MP) (Ref. 23) grid used for Brillouin-zone integrations ensured highly converged results (to about 1 meV per formula unit). We use 16, 24, 8, and 6 k-points to

perform the geometrical optimizations of $MgWO_4$ with symmetry $P2/c$ (wolframite), $P\bar{1}$, $C2/c$, and *Cmca*, respectively. For $MnWO_4$ we performed spin density calculations and we found that the antiferromagnetic configuration was the most stable one. For the Brillouin zone integrations we used 16 k-points with an MP grid of (4, 4, 4) for the analyzed structures. At each selected volume, the structures were fully relaxed to their equilibrium configuration through the calculation of the forces on atoms and the stress tensor—see Ref. 24. In the relaxed equilibrium configuration, the forces are less than 0.004 eV/Å and the deviation in the stress tensor from a diagonal hydrostatic form is less than 1 kbar (0.1 GPa). The highly converged results on forces are required for the calculation of the dynamical matrix using the direct force constant approach (or supercell method).[25] The construction of the dynamical matrix at the Γ point involves separate calculations of the forces in which a fixed displacement from the equilibrium configuration of the atoms within the *primitive* cell is considered. Symmetry aids by reducing the number of such independent distortions, reducing the amount of computational effort in the study of the analyzed structures considered in our work. Diagonalization of the dynamical matrix provides both the frequencies of the normal modes and their polarization vectors, it allows us to identify the irreducible representation and the character of the phonon modes at the zone center. The calculations performed for $ZnWO_4$ and $CdWO_4$ and their results have been described in detail in Refs. 6 and 8.

IV. RESULTS AND DISCUSSION

A. XRD studies

A sequence of the evolution with pressure of selected XRD patterns of $MgWO_4$ is shown in Fig. 2. All the Bragg reflections can be indexed up to 17.1 GPa according to the wolframite structure. At this pressure additional peaks appear (see Figs. 2 and 3); e.g., the peak located around 2θ=7.2°. As pressure increases these and extra peaks grow in intensity up to 27.4 GPa. This fact suggests the onset of a phase transition at 17.1 GPa from the wolframite structure to a HP one. At 31 GPa an additional peak appears. The appearance of this peak is followed by the appearance of two more at 35.1 GPa and extra ones up to 41.1 GPa. This fact points out to the onset of a second phase transition at 31 GPa to a phase that we will denote as phase III. Both transitions are reversible as it can be seen on the diffraction pattern collected at 0.2 GPa after pressure release. This pattern is similar to the one obtained at 0.6 GPa before compression. The only difference is the stress-induced peak broadening which is not fully recovered upon decompression. In $ZnWO_4$ similar changes in the diffraction patterns than in $MgWO_4$ have been found (see Fig. 4), with a phase transition onset at about 16.7 GPa, pointing to a similar phase transition than in $MgWO_4$.

Regarding the crystalline structure of the postwolframite phase, in both compounds we can tell that the diffraction patterns suggest a reduction in the crystal symmetry after the phase transition. Given the small number of reflections and their broad nature we have not been able to perform a Rietveld refinement for the HP phases. However, a Le Bail

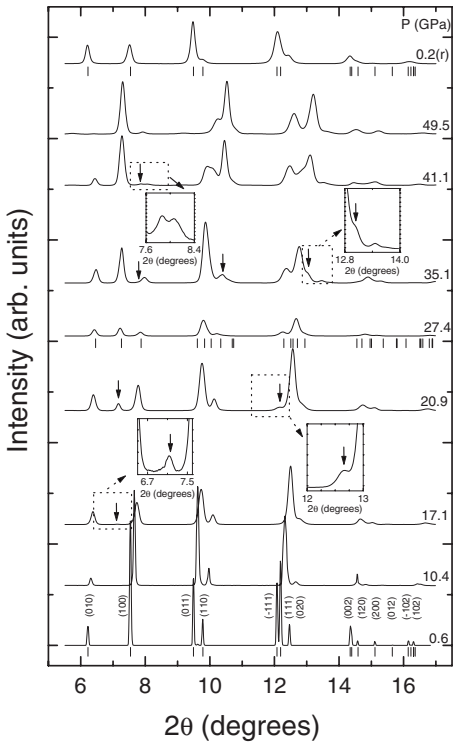

FIG. 2. Selection of $MgWO_4$ ADXRD patterns at different pressures from 0.6 to 49.5 GPa. The insets show enlarged areas of the diffraction patterns to illustrate the appearance of weak peaks. The vertical bars indicate the calculated positions of the reflections of the wolframite and triclinic structures. Most intense peaks of each structure are also labeled. The arrows indicate the appearance of peaks of HP phases.

analysis of the diffraction patterns measured for $MgWO_4$ at 27.4 GPa indicated that its first HP phase has a triclinic $P\bar{1}$ symmetry with Z=2, in agreement with previous Raman studies from intermediate wolframite structures in related compounds.[26] In particular, at 27.4 GPa we obtain the following unit-cell parameters for the potential triclinic polymorph of $MgWO_4$: a=4.459(9) Å, b=5.431(9) Å, c =4.832(9) Å, α=91.4(5)°, β=89.7(5)°, and γ=91.7(5)°. Therefore, this phase resembles the structure of $CuWO_4$

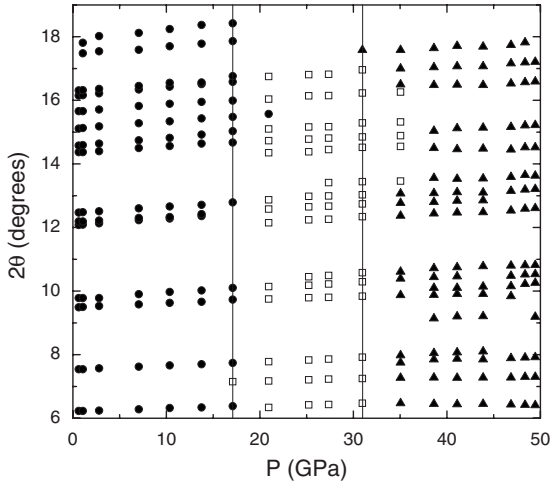

FIG. 3. $MgWO_4$ peaks evolution with pressure. Circles: wolframite, squares: triclinic phase, triangles: phase III. The vertical lines indicate the onset of transitions.

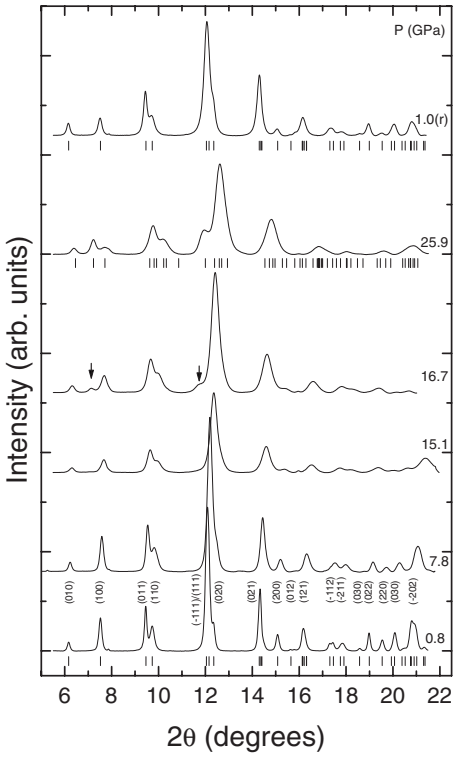

FIG. 4. Selection of $ZnWO_4$ ADXRD patterns at different pressures from 0.7 to 25.9 GPa. The vertical bars indicate the calculated positions of the reflections of the wolframite and triclinic structures. Most intense peaks of each structure are also labeled. The arrows indicate the appearance of peaks of HP phases.

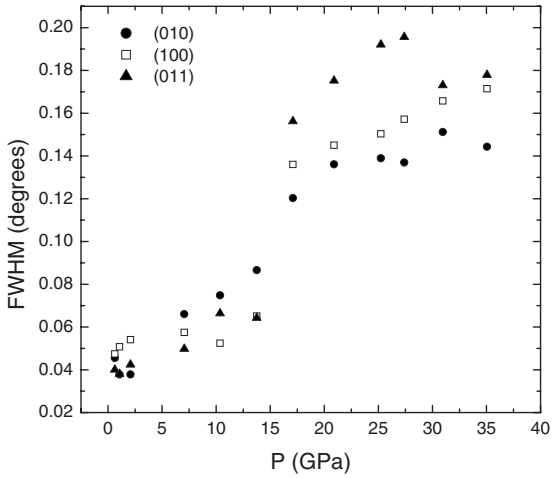

FIG. 5. Evolution with pressure for the FWHM of three independent Bragg peaks in $MgWO_4$.

(Ref. 27) and $FeMoO_4$-II,[28] a distorted version of wolframite, which is topologically related to it. Note that the triclinic space group is a subgroup of the monoclinic space group and consequently the proposed transition appears to be continuous. This is consistent with our finding that the coordination of the Mg and W atoms does not change at the transition. Comparing both structures in Fig. 1, it can be seen that the phase transition mainly consists on a movement of the oxygen and Mg atoms, implying a rotation of the MgO_6 octahedron and a distortion of it. This distortion is enough to reduce the symmetry to triclinic. Basically, the proposed transition involves a tilting and distortion of the MgO_6 octahedra, which produces a local symmetry breakdown into the triclinic symmetry. In the triclinic phase, the Mg atoms have a more irregular coordination compared with wolframite. As we will show later, a similar structure is predicted by our *ab initio* calculations for the HP phase of $MgWO_4$. Consequently, the triclinic structure here proposed is the most plausible candidate for HP $MgWO_4$. Note that this triclinic structure is not the same as the triclinic phase synthesized at high-temperature conditions.[29]

Another evidence supporting the occurrence of a phase transition at 17.1 GPa is given in Fig. 5, where the full-width at half maximum (FWHM) of three Bragg peaks is represented as a function of pressure. A steep increase in the FWHM is seen at 17.1 GPa, coinciding with the transition onset. This fact can be explained by comparing the diffraction patterns of both structures. Given the group-subgroup relationship between space groups $P2/c$ and $P\bar{1}$, the wolframite peaks can be also accounted for with the new triclinic structure. However, the triclinic distortion gives rise to a contribution from extra peaks that split from the original wolframite peaks causing part of the observed peak broadening. This broadening is also stress-induced as shown in other tungstates[9,10] regardless the pressure medium used in the experiments. To close the discussion of the XRD experiments in $MgWO_4$, we would like to add that the crystal structure of phase III is left unsolved despite attempts made to determine it. However, the reduction in number of peaks suggests an increase in the symmetry of the crystal. As we will describe latter (Sec. IV D), this fact qualitatively agrees with theoretical predictions.

For $ZnWO_4$, our XRD experiments suggest that the HP phase has the same triclinic structure as HP $MgWO_4$. In particular, at 25.9 GPa we obtain the following unit-cell parameters for the triclinic polymorph of $ZnWO_4$: a=4.529(9) Å, b=5.407(9) Å, c=4.418(9) Å, α=91.2(5)°, β=87.1(5)°, and γ=91.8(5)°. The transformation to this phase is apparently in contradiction with previous Raman-spectroscopy experiments,[8] which reported the onset of a phase transition to a monoclinic β-fergusonite-type phase ($C/2c$) beyond 30.6 GPa. However, the onset of the transition here detected (16.7 GPa) is very close to the pressure were a domain formation was observed in single-crystalline $ZnWO_4$ together with a relative change in the Raman peak intensities.[8] A possible explanation for the non detection of the transition at 16.7 GPa in previous experiments can be the use of different pressure-transmitting media (Ar in Raman experiments and silicone oil in present experiments). According with *ab initio* calculations the triclinic $P\bar{1}$ structure is energetically competitive with the wolframite (see Fig. 4 of Ref. 8) and β-fergusonite-type structures. Therefore the non-hydrostatic stresses induced by the use of silicone oil as pressure medium could favor the transition to a metastable triclinic structure. In our ADXRD experiments the maximum pressure reached is below the onset of the transition to the $C2/c$ structure, which prevents us to make any conclusions about the structure of this phase. This explanation is also consistent with the rich polymorphism observed in other orthotung-

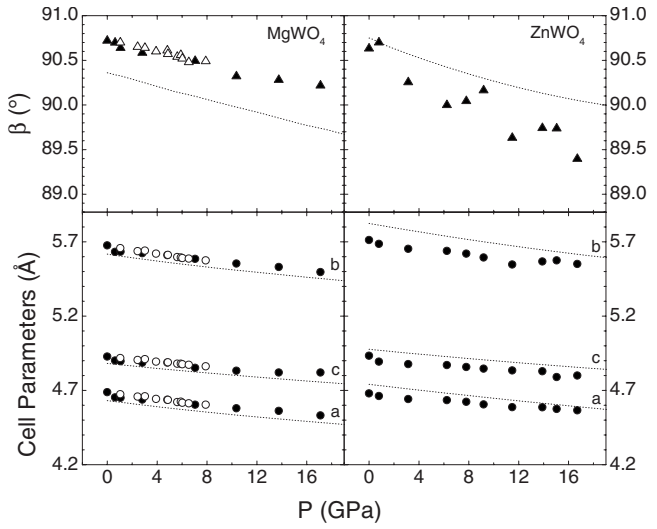

FIG. 6. Lattice-parameters evolution of $MgWO_4$ and $ZnWO_4$ on the monoclinic structure. Solid symbols: this work. Empty symbols: Ref. 11. Lines: *ab initio* calculations.

states under compression, e.g., $BaWO_4$ and $PbWO_4$ (Ref. 30) and the fact that kinetics has an important effect in their pressure-driven phase transitions. Note that the triclinic structure was also observed in $CdWO_4$ as an intermediate phase between the low-pressure wolframite structure and the HP β-fergusonite phase.[6] Therefore, in addition to $MgWO_4$ and $CdWO_4$, the triclinic phase can be also pressure-induced in $ZnWO_4$ several gigapascal below the β-fergusonite phase.

From the analysis of our XRD data, we extracted the pressure dependence of the lattice parameters for both wolframite $MgWO_4$ and $ZnWO_4$. These results are summarized in Fig. 6. This behavior is in agreement with the low-pressure behavior reported by Macavei *et al.*[11] from single crystal studies up to 8 GPa. In Fig. 7 we report the evolution of the unit-cell volumes of $MgWO_4$ and $ZnWO_4$ obtained from our experiments as well as previous data[11] for $MgWO_4$, $MnWO_4$ and $CdWO_4$. For $MgWO_4$ our data are in good agreement with single-crystal diffraction data within the pressure range covered by these measurements.[11] We have analyzed the volume changes using a third-order Birch–Murnaghan EOS.[31] The EOS parameters for $MgWO_4$ [$ZnWO_4$] are: $V_0=131.1(3)$ Å^3 [132.9(5)], $B_0=160(13)$ GPa [145(6)], and $B_0'=4.5(3)$ [6.6(9)], these parameters being the zero-pressure volume, bulk modulus, and its pressure derivative, respectively.

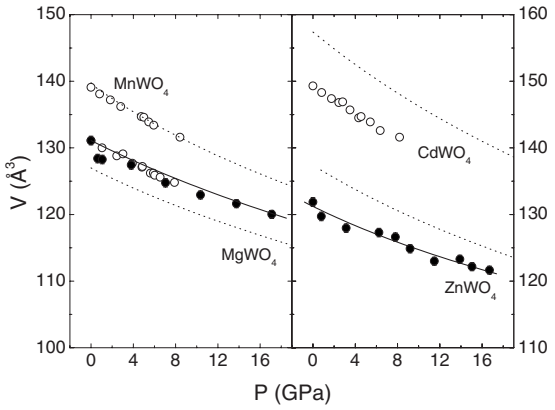

FIG. 7. EOS for wolframite $MnWO_4$, $MgWO_4$, $CdWO_4$, and $ZnWO_4$. The empty (filled) circles correspond to Macavei *et al.* (Ref. 11) (present work), the dotted (solid) lines correspond to *ab initio* calculations (fitted EOS).

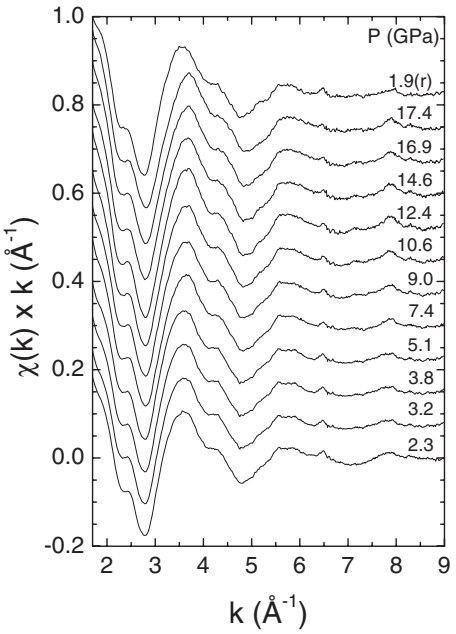

FIG. 8. $ZnWO_4$ EXAFS spectra for several pressures from 2.3 to 17.4 GPa. The spectrum marked as 1.9(r) corresponds to the one obtained on pressure release.

B. X-ray absorption measurements

Figure 8 shows a selection of extended x-ray absorption fine structure (EXAFS) signals measured in $ZnWO_4$ at different pressures. The EXAFS signal remains stable under pressure, showing a slight displacement toward higher k values as pressure is increased due to the shortening of the Zn–O distances. In order to analyze these results, we obtained the pair-pseudodistribution function (PPDF) by Fourier transformation (FT) of the EXAFS oscillations in the (1.2, 9) k range, using a Bessel-type ($Z=4$) apodization window (see Fig. 9). The main peak is associated to the first oxygen neighbor shell. The six distances in the ZnO_6 octahedron can be grouped in one short (x4) and one long distance (x2). The position at about 1.42 Å of this broad peak—0.8 Å FWHM—slowly changes with pressure pointing toward smaller R values with almost identical shape and FWHM. The fit to the main peak (see Fig. 9) has been made with the WINXAS program and calculating the corresponding phases and amplitudes with the *ab initio* FEFF 8.6 code (Ref. 32) for multiple-scattering x-ray absorption fine structure.

From the analysis of the EXAFS data we obtained the evolution with pressure of the Zn–O distances. These results are shown in Fig. 10 together with those obtained from our diffraction measurements in the wolframite phase-considering for simplicity no variation in the Wychoff positions with pressure-calculations and *ab initio* calculations. In particular, we found that the different methods give a qualitatively similar behavior. In both wolframites there is a noticeable difference in the compressibility shown under pres-

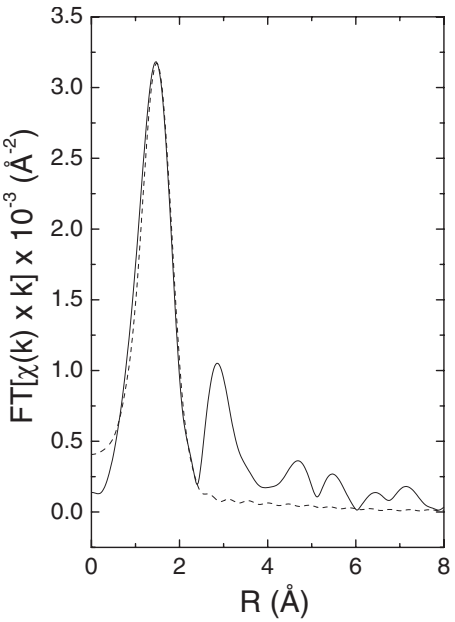

FIG. 9. PPDF obtained by Fourier transformation of the EXAFS signal at 3.2 GPa. The dot line corresponds to the calculation.

sure between the W–O and the A–O distances. The compressibility of the later is at least three times the one of the former. Therefore, it can be considered that WO_6 octahedra behave as rigid units while MgO_6 (ZnO_6) octahedra account for most of the crystal compressibility. If we compare the evolution for the distances calculated and those obtained through ADXRD experiments it can be pointed out that for W–O bonds in $ZnWO_4$, the assumption that Wychoff positions do not change with pressure seems to be a good approximation. However, this simplification does not work so well for the Zn–O distances. In the case of the $MgWO_4$ the same approximation appears to work well below 6 GPa, since bond distances obtained are similar to those obtained from a full structural refinement.[11] The only differences are seen for the longest bond that shows to be more compressible than in the *ab initio* calculations and our ADXRD results.

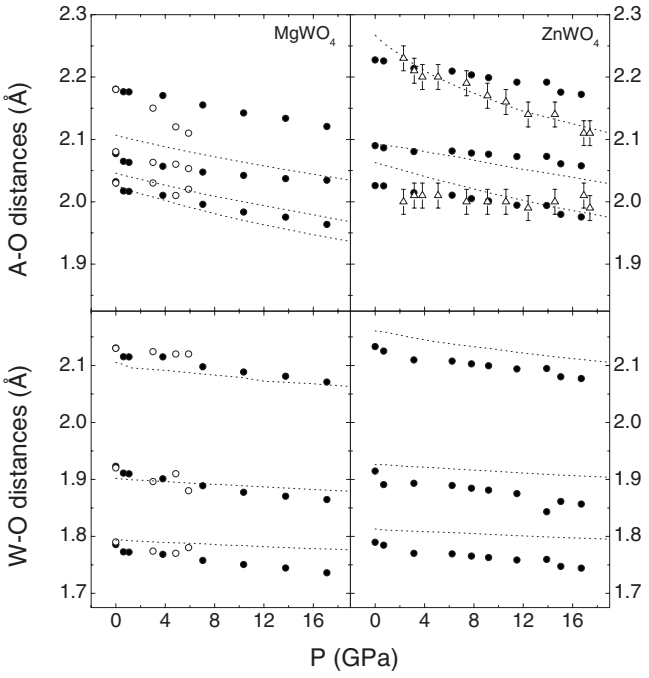

FIG. 10. A–O and W–O distances for the $MgWO_4$ and $ZnWO_4$ wolframites. The empty circles are the distances obtained by Macavei *et al.* (Ref. 11). The solid ones are the distances obtained in the present work through the ADXRD study. The triangles correspond to the distances obtained with EXAFS. The dotted lines are the *ab initio* calculations.

Regarding the calculations, even though the theoretical Mg–O distances differ in absolute value from the experimental ones, the bond compressibilities found are in good accordance with ADXRD results. In the case of the W–O distances of $MgWO_4$, the agreement between the experiments and the calculations is better for the compressibility of the longest W–O distance than for the shortest ones. The largest Zn–O distance obtained through EXAFS is in very good agreement with the one obtained from the calculations as well as with the high compressibility of the A–O bond found by Macavei *et al.*[11] in several wolframites. This fact points out that considering the Wychoff positions as constant is not the best approximation meaning that the ZnO_6 octahedra are modified under pressure. Regarding the shortest distance obtained from EXAFS, it is slightly underestimated and almost does not change with pressure. This can be caused by the fact that this distance is assumed as an average of four different distances, having apparently little influence in the position of the FT peak.

To close this section, we would like to mention now that we have not observed any detectable change in the x-ray absorption near edge structure (XANES) signal in $ZnWO_4$ under HP up to 17.4 GPa. Since XANES originates from multiple scattering of photoelectrons, it is very sensitive to changes in symmetry around the absorbing atom. Thus the unchanged XANES signal indicates that at the phase transition (onset at 16.7 GPa) the ZnO_6 octahedra are only slightly modified and the Zn–O coordination not modified. This conclusion is in agreement with the wolframite-triclinic transition proposed from XRD studies.

C. Raman measurements

In contrast with $CdWO_4$ and $ZnWO_4$, Raman spectroscopy data have not been reported up to now in $MgWO_4$. According to group theory, the wolframite structure presents at the Γ point 18 Raman active modes ($8A_g+10B_g$) and 18 IR ones ($8A_u+10B_u$). In this kind of compounds,[8,26] due to the difference in valence and mass between W^{6+} atoms and A^{2+}, the lattice dynamics can be understood assuming two kinds of modes. Six of them related with motions inside the covalently bounded WO_6 octahedra called internal and other modes originated as motions of the A cations against the WO_6 units named external. The internal modes are at higher frequencies than the external ones and usually there is a phonon gap between them.[6,8] According to our calculations the internal modes of the $MgWO_4$ are the A_g modes at 420.4, 551.6, 713.2, and 916.8 cm^{-1} and the B_g modes at 683.9 and 808.5 cm^{-1}.

The Raman spectrum measured at ambient conditions for $MgWO_4$ is presented in Fig. 11. We have been able to

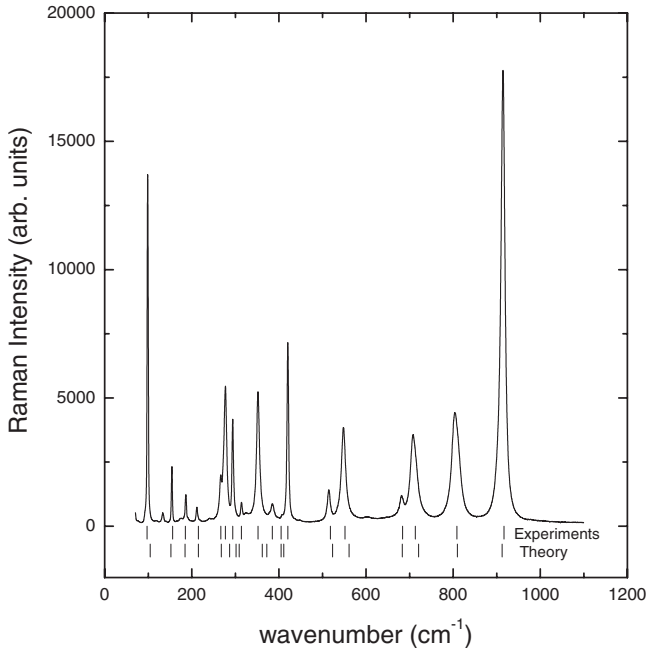

FIG. 11. Raman spectrum of the $MgWO_4$ at ambient conditions. The theoretical and experimental positions of the phonons are shown.

observe the 18 Raman modes of $MgWO_4$ being their frequencies (ω) in good agreement with our calculations (see Table I). The assignment of the modes was done based in the calculations and the similarities between the Raman spectra of $MgWO_4$, $CdWO_4$, and $ZnWO_4$.[6,8] Typical of the Raman spectrum of wolframite is the strong phonon found at 916.6 cm^{-1}. This phonon corresponds to a symmetric A_g internal vibration of the WO_6 octahedron and appears near 900 cm^{-1} in all the studied wolframites. The corresponding antisymmetric A_g vibration is the one found at 713.2 cm^{-1}. In Table I, the theoretical pressure coefficient and Grüneisen parameters for each phonon are included ($\gamma=(B_0/\omega)\times(\partial\omega/\partial P)$, calculated assuming $B_0=141$ GPa). The agreement obtained between experiments and calculations at ambient pressure validates our theoretical predictions for HP. In Table II the calculated IR active modes as well as their pressure coefficients and Grüneisen parameters are shown for completeness. The agreement with ambient pressure experiments[33] is good for the modes that have been measured with the exception of B_u mode measured at 845 cm^{-1}. In spite of this difference, *ab initio* calculations have shown to be an efficient tool to study the HP lattice-dynamics of tungstates.[6,8] According with them, there are three IR modes that soften upon compression in $MgWO_4$. This mode softening is consistent with the HP monoclinic-triclinic transition.

TABLE I. *Ab initio* calculated and experimental Raman frequencies (1 bar) as well as calculated pressure coefficients, and Grüneisen parameters of the Raman modes in wolframite $MgWO_4$.

	Theory			Experiment
Mode	ω (cm^{-1})	$d\omega/dP$ (cm^{-1} GPa)	γ	ω (cm^{-1})
B_g	104.34	0.80	1.38	97.4
A_g	152.11	0.24	0.30	155.9
B_g	184.60	0.44	0.45	185.1
B_g	215.29	0.62	0.54	215.0
B_g	267.66	1.01	0.71	266.7
A_g	286.98	0.51	0.34	277.1
A_g	301.55	1.93	1.17	294.1
B_g	308.83	1.79	1.05	313.9
A_g	361.77	4.20	2.03	351.9
B_g	372.27	3.90	1.85	384.8
B_g	405.16	5.42	2.31	405.2
A_g	411.27	1.67	0.75	420.4
B_g	523.38	3.31	1.15	518.1
A_g	560.94	3.33	1.08	551.6
B_g	683.23	4.34	1.15	683.9
A_g	720.73	3.34	0.85	713.2
B_g	809.79	4.14	0.94	808.5
A_g	912.50	3.61	0.73	916.8

TABLE II. *Ab initio* calculated and experimental IR frequencies (1 bar) as well as the calculated pressure coefficients, and Grüneisen parameters of the IR in wolframite $MgWO_4$.

	Theory			Experiment
Model	ω (cm^{-1})	$d\omega/dP$ (cm^{-1}/GPa)	γ	ω (cm^{-1})
B_u	0	⋯	⋯	⋯
A_u	1.77	⋯	⋯	⋯
B_u	1.7	⋯	⋯	⋯
B_u	193.74	−0.23	−0.20	194
B_u	241.54	−0.77	−0.62	⋯
B_u	268.40	−0.76	−0.56	268
A_u	278.94	1.02	0.69	291
B_u	315.73	3.62	2.01	⋯
A_u	331.98	0.30	0.17	⋯
A_u	341.78	1.58	0.85	338
B_u	366.94	4.97	2.33	382
A_u	445.89	4.30	1.70	408
B_u	482.75	5.18	1.89	483
A_u	519.05	4.39	1.51	⋯
B_u	575.66	3.38	1.07	534
A_u	685.70	3.47	0.92	715
B_u	777.94	3.30	0.78	845
A_u	869.40	3.22	0.68	899

D. Theoretical results

In order to help with the interpretation of our experimental results, *ab initio* total-energy and lattice-dynamics calculations were performed for $MgWO_4$. Similar calculations were performed for $MnWO_4$ and previously for $CdWO_4$ (Ref. 6) and $ZnWO_4$.[8] These results will be systematically compared with the bulk of experimental results available for wolframite tungstates. For $MgWO_4$, along with the wolframite structure, we have considered other structures on account of their observation or postulation in previous HP works for related compounds: $CuWO_4$-type ($P\bar{1}$), orthorhombic-disorder wolframites ($A2_1am$, *Pmma*, *Pbam*, *Pbcm*, *Pbcn*, *Pbnm*, *Cmcm*, and *Cmca* from $LaTaO_4$, $CaRhIn_4$, $YbCoB_4$, $BaUO_4$, $NaScCl_4$, $MgSeO_4$, $CaSO_4$, and $PbWO_4$, respectively), M-fergusonite ($I2/a$), M′-fergusonite ($P2_1/c$), β-fergusonite ($C2/c$), monoclinic-disorder wol-

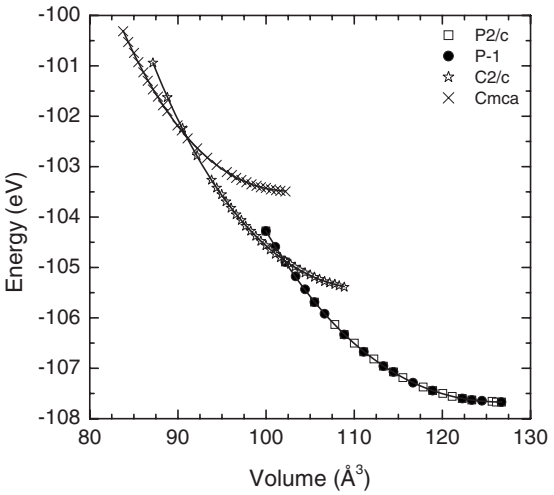

FIG. 12. *Ab initio* energy vs volume curves for the most stable structures found for the $MgWO_4$ calculation.

framites (Pc, $P2/m$, $C2/m$, and $P2_1/n$ from $KAuCl_4$, $CrAuTe_4$, $CrPS_4$, and $AgMnO_4$, respectively), and scheelite ($I4_1/a$). Figure 12 shows the energy versus volume curves for the most competitive structures. The common tangent construction enables to deduce the transition and equilibrium pressures.[34] In the figure we only reported those structures that play a relevant role in the HP structural behavior of $MgWO_4$. According to the calculations wolframite ($P2/c$) is the most stable structure at ambient pressure. The calculated lattice parameters for this structure are: a=4.6332 Å, b=5.6197 Å, c=4.8831, and β=90.36. These parameters are slightly smaller than the experimental values. The differences are within the typical reported systematic errors in DFT-LDA calculations. The calculated EOS of wolframite $MgWO_4$ is given by the following parameters V_0=127.2 Å^3, B_0=161 GPa, and B_0'=4.2. They were obtained using the Birch–Murnaghan EOS.[31] Above 35.4 GPa the calculations predict that the most stable structure would be a β-fergusonite one ($C2/c$). Its lattice parameters and Wychoff positions are in Table III together with a higher-symmetry orthorhombic structure ($Cmca$) predicted to become stable beyond 48 GPa as well as the structural information about wolframite. The proposed transition to the β-fergusonite structure is possible given the evidence available in $CdWO_4$ and $ZnWO_4$.[6,8] The stabilization of the orthorhombic structure involves a coordination increase for Mg from 6 to 10. The coordination of W remains unaltered. The appearance of this structure is in agreement with the HP systematic developed by Bastide[1] and with the structural sequence found in other tungstates.[35] The confirmation of the existence of the β-fergusonite and $Cmca$ structures is waiting for future experiments.

Regarding the triclinic $P\bar{1}$ structure, the calculations also predict that in the pressure range where it was experimentally observed, it is energetically competitive with wolframite. This means that possible uniaxial stresses induced by the use of a pressure medium like silicone oil could be enough to induce a phase transition from the wolframite structure to the triclinic one. This fact could probably be the cause of the finding of the triclinic phase between the wolframite and β-fergusonite phases in $MgWO_4$ and $ZnWO_4$. In Table III we report the calculated structural information for the $P\bar{1}$ structure at 29 GPa. The agreement with the experimental values is good.

As we mentioned above, calculations have been performed for the low-pressure phase of $MnWO_4$. Since this compound could be magnetic due to the presence of the Mn cation, we considered different magnetic configurations. We found the low-pressure phase of $MnWO_4$ to have a wolframite structure with an antiferromagnetic configuration. In this configuration, Mn has a magnetic moment of 4.319 μB while in the ferromagnetic configuration is 4.356 μB. The structural information for this phase is summarized in Table IV. The agreement with the literature[11] is good. For this phase we also calculated its EOS obtaining the following

TABLE IV. Unit-cell parameters and Wychoff positions of $MnWO_4$ at ambient pressure.

a=4.7958 Å, b=5.8007 Å, c=5.0254 Å, β=90.972°				
Atom	Site	x	y	z
Mn	2f	0.5	0.6734	0.25
W	2e	0	0.1760	0.25
O1	4g	0.2137	0.1068	0.0636
O2	4g	0.2561	0.3726	0.3977

TABLE III. Structural information of the calculated structures for $MgWO_4$.

	$P2/c$ (1 atm)	$P\bar{1}$ (29.0 GPa)	$C2/c$ (35.4 GPa)	$Cmca$ (48 GPa)
a	4.6332	4.414	6.123	7.131
b	5.6197	5.3632	9.183	10.375
c	4.8831	4.689	4.744	4.974
α	90.00	90.00	90.00	90.00
β	90.36	89.34	131.10	90.00
γ	90.00	90.00	90.00	90.00
Mg	2f (0.5, 0.6691, 0.25)	2i (0.5, 0.6729, 0.25)	4e (0, 0.3272, 0.25)	8e (0.25, 0.3585, 0.25)
W	2e (0, 0.1823, 0.25)	2i (0, 0.1969, 0.25)	4e (0, 0.8801, 0.25)	8f (0, 0.1064, 0.2599)
O_1	4g (0.2171, 0.8955, 0.4360)	2i (0.2577, 0.5982, 0.5761)	8f (0.2887, 0.4542, 0.3852)	8e (0.25, 0.1743, 0.25)
O_2	4g (0.2547, 0.3772, 0.4005)	2i (0.2377, 0.0939, 0.5668)	8f (0.7186, 0.2077, 0.2583)	8f (0, 0.2770, 0.0502)
O_3		2i (0.2577, 0.4018, 0.0761)		8d (0.3375, 0, 0)
O_4		2i (0.2377, 0.9061, 0.0669)		8f (0, 0.4208, 0.3764)

TABLE V. Bulk modulus and unit-cell volume for different wolframites obtained by *ab initio* calculations, experiments, and phenomenological estimates.

	Volume ($Å^3$)		Bulk modulus (GPa)			
Compound	Experimental values	*Ab initio calculations*	Previous experiments	Our experiments	*Ab initio calculations*	Phenomenological estimates
$MgWO_4$	131.1–132[a]	127.2	144[a]	160(13)	161	141
$ZnWO_4$	132.9	137.4	153[b]–161[c]	145(6)	140	140
$MnWO_4$	138.8[a]	139.8	131[a]		125	125
$CdWO_4$	149.3[a]	157.4	136[a]		125	120

[a]Reference 11.
[b]Reference 39.
[c]Reference 40.

parameters: $V_0=157.4$ $Å^3$, $B_0=125$ GPa, and $B_0'=4.3$. The bulk modulus agrees well with the previously reported experimental value.[11]

To conclude we would like to compare the different compressibilities reported for $MgWO_4$, $MnWO_4$, $CdWO_4$ and $ZnWO_4$. A summary of their bulk moduli and unit-cell volume are given in Table V. It is straightforward to see there, that there is an inverse correlation between the volume and the bulk modulus. As expected the densest compounds are the less compressible. It can be also seen that our experimental values agree with previous values within 10%. The same conclusion can be extracted for our calculations. Indeed calculations agree very well with the experiments. In addition, all the results show that the linear combination of atomic orbitals approach leads to unreasonable large values for the bulk modulus of $ZnWO_4$ ($B_0=257$ GPa).[36] Some additional insight on the compressibility of wolframites can be extracted from their polyhedral compressibility. As we discussed above, W–O bonds are much more rigid than A–O bonds. Then, the compression of wolframite can be attributed dominantly to changes in the A–O bond lengths. The same trend has been found in scheelite-structured orthotungstates, orthomolybdates, and orthogermanates,[35,37–40] leading to a phenomenological rule that correlates the bulk modulus with the inverse of the A–O distance. If the same rule is applied to wolframite, we estimate the bulk modulus given in the right hand-side column of Table V. As can be seen there, the estimated values reproduce the tendency followed by the bulk compressibility of wolframites but slightly underestimate the bulk modulus. However, we think, the phenomenological rule[35] can be used to roughly estimate B_0 for unstudied wolframites like $FeWO_4$ (134 GPa), $NiWO_4$ (141 GPa), and $CoWO_4$ (137 GPa). Finally, the different compressibility of AO_6 and WO_6 octahedra also explains that the compaction of wolframite is more important in the *b*-axis than in other axes. Basically, it is related to the different linking of octahedral units along different crystallographical directions.

V. CONCLUSIONS

By means of XRD and absorption experiments and *ab initio* calculations we have studied the structural properties of different wolframite compounds up to 50 GPa. For $MgWO_4$ we have found evidences of two pressure-induced phase transitions at 17.1 and 31 GPa. A phase transition was detected in $ZnWO_4$ at 16.7 GPa, a lower pressure than that of the previously reported one[8] (30 GPa). Apparently, the first transition involves a symmetry-reduction in the crystal from monoclinic to triclinic. The proposed-structure for the HP phase is similar to that of $CuWO_4$. We also report an EOS for $MgWO_4$, $MnWO_4$, $ZnWO_4$, and $CdWO_4$. Information on the bond compressibility is reported too and related with the bulk compressibility of wolframite. Raman measurements and lattice-dynamics calculations are also presented for $MgWO_4$. Most of its modes have been identified and their Grüneisen parameters reported. Finally, different magnetic configurations have been considered for wolframite $MnWO_4$, being found that it is antiferromagnetic.

ACKNOWLEDGMENTS

ADXRD experiments carried out at the Diamond Light Source (I15 beamline, Proposal No. 683). The authors thank A. Kleppe for technical support. Research financed by Spanish MEC (Grant Nos. MAT2007-65990-C03-01/03 and CSD-2007-00045) as well as Mexican CONACyT (Grant Nos. J-59853-F and J-83247-F). J.R.-F. (R.L.-P.) thanks the MEC support through FPI (FPU) program. We thank SOLEIL for granting us beamtime and the ODE staff for technical assistance.

[1]D. Errandonea and F. J. Manjon, Prog. Mater. Sci. **53**, 711 (2008) and references therein.
[2]D. Errandonea, D. Martínez-García, R. Lacomba-Perales, J. Ruiz-Fuertes, and A. Segura, Appl. Phys. Lett. **89**, 091913 (2006).
[3]A. W. Sleight, Acta Crystallogr., Sect. B: Struct. Crystallogr. Cryst. Chem. **28**, 2899 (1972).
[4]R. O. Keeling, Acta Crystallogr. **10**, 209 (1957).
[5]A. Jayaraman, S. Y. Wang, and S. K. Sharma, Curr. Sci. **69**, 44 (1995).
[6]R. Lacomba-Perales, D. Errandonea, D. Martinez-Garcia, P. Rodríguez-Hernández, S. Radescu, A. Mujica, A. Muñoz, J. C. Chervin, and A. Polian, Phys. Rev. B **79**, 094105 (2009).
[7]A. Perakis, E. Sarantapoulou, and C. Raptis, High Press. Res. **18**, 181 (2000).
[8]D. Errandonea, F. J. Manjon, N. Garro, P. Rodriguez-Hernandez, S. Radescu, A. Mujica, A. Muñoz, and C. Y. Tu, Phys. Rev. B **78**, 054116 (2008).
[9]D. Errandonea, M. Somayazulu, and D. Häusermann, Phys. Status Solidi B **235**, 162 (2003).
[10]D. Errandonea, Phys. Status Solidi B **242**, R125 (2005).
[11]J. Macavei and H. Schulz, Z. Kristallogr. **207**, 193 (1993).
[12]Y. Shen, R. S. Kumar, M. Pravica, and M. F. Nicol, Rev. Sci. Instrum. **75**, 4450 (2004).
[13]D. Errandonea, Y. Meng, M. Somayazulu, and D. Häusermann, Physica B **355**, 116 (2005).
[14]H. K. Mao, J. Xu, and P. M. Bell, J. Geophys. Res. **91**, 4673 (1986).
[15]R. Lacomba-Perales, J. Ruiz-Fuertes, D. Errandonea, D. Martínez-García, and A. Segura, EPL **83**, 37002 (2008).

[16]G. Kresse and J. Hafner, Phys. Rev. B **47**, 558 (1993).
[17]G. Kresse and J. Hafner, Phys. Rev. B **49**, 14251 (1994).
[18]G. Kresse and J. Furthmüller, Phys. Rev. B **54**, 11169 (1996).
[19]J. P. Perdew and A. Zunger, Phys. Rev. B **23**, 5048 (1981).
[20]J. Perdew, K. Burke, and M. Ernzerhof, Phys. Rev. Lett. **78**, 1396 (1997).
[21]P. E. Blöchl, Phys. Rev. B **50**, 17953 (1994).
[22]G. Kresse and D. Joubert, Phys. Rev. B **59**, 1758 (1999).
[23]H. J. Monkhorst and J. D. Pack, Phys. Rev. B **13**, 5188 (1976).
[24]F. J. Manjón, D. Errandonea, N. Garro, J. Pellicer-Porres, P. Rodríguez-Hernández, S. Radescu, J. López-Solano, A. Mujica, and A. Muñoz, Phys. Rev. B **74**, 144111 (2006).
[25]K. Parlinski, computer code PHONON. See: http://wolf.ifj.edu.pl/phonon.
[26]A. Jayaraman, G. A. Kourouklis, L. G. Van Uitert, W. H. Grodkiewicz, and R. G. Maines, Physica A **156**, 325 (1989).
[27]L. Kihlborg and E. Gebert, Acta Crystallogr., Sect. B: Struct. Crystallogr. Cryst. Chem. **26**, 1020 (1970).
[28]A. W. Sleight, B. L. Chamberland, and J. F. Weiher, Inorg. Chem. **7**, 1093 (1968).
[29]R. Lacomba-Perales, D. Martínez-García, D. Errandonea, Y. Le Godec, J. Philippe, and G. Morard, High Press. Res. **29**, 76 (2009).
[30]J. R. Günter and M. Amberg, Solid State Ionics **32–33**, 141 (1989).
[31]F. Birch, J. Geophys. Res. **83**, 1257 (1978).
[32]J. J. Rehr, R. C. Albers, and S. I. Zabinsky, Phys. Rev. Lett. **69**, 3397 (1992).
[33]L. J. Burcham and I. E. Wachs, Spectrochim. Acta, Part A **54**, 1355 (1998).
[34]A. Mujica, A. Rubio, A. Muñoz, and R. J. Needs, Rev. Mod. Phys. **75**, 863 (2003).
[35]D. Errandonea, J. Pellicer-Porres, F. J. Manjón, A. Segura, Ch. Ferrer-Roca, R. S. Kumar, O. Tschauner, P. Rodríguez-Hernández, J. López-Solano, S. Radescu, A. Mujica, A. Muñoz, and G. Aquilanti, Phys. Rev. B **72**, 174106 (2005).
[36]R. A. Evarestov, A. Kalinko, A. Kuzmin, M. Losev, and J. Purans, Integr. Ferroelectr. **108**, 1 (2009).
[37]D. Errandonea, R. S. Kumar, X. Ma, and C. Y. Tu, J. Solid State Chem. **181**, 355 (2008).
[38]D. Errandonea, R. S. Kumar, L. Gracia, A. Beltrán, S. N. Achary, and A. K. Tyagi, Phys. Rev. B **80**, 094101 (2009).
[39]Y. V. Pisarevskii, I. M. Silvestrova, R. Voszka, A. Peter, I. Foldvari, and J. Janszky, Phys. Status Solidi A **107**, 161 (1988).
[40]D. M. Trots, A. Senyshyn, L. Vasylechko, R. Niewa, T. Vad, V. B. Mikhailik, and H. Kraus, J. Phys.: Condens. Matter **21**, 325402 (2009).